Research Article | Vol. 26, No. 18 | 3 Sep 2018 | OPTICS EXPRESS A750
Optics EXPRESS

Optical design of spectrally selective interlayers for perovskite/silicon heterojunction tandem solar cells

K. BITTKAU,[1,*] T. KIRCHARTZ,[1,2] AND U. RAU[1]

[1]*IEK5 – Photovoltaik, Forschungszentrum Jülich GmbH, 52425 Jülich, Germany*
[2]*Faculty of Engineering and CENIDE, University of Duisburg–Essen, Carl-Benz-Straße 199, 47057 Duisburg, Germany*
**k.bittkau@fz-juelich.de*

Abstract: Monolithic perovskite/c-Si tandem solar cells have the potential to exceed the Shockley-Queisser limit for single junction solar cells. However, reflection losses at internal interfaces play a crucial role for the overall efficiency of the tandem devices. Significant reflection losses are caused by the charge selective contacts which have a significantly lower refractive index compared to the absorber materials. Here, we present an approach to overcome a significant part of these reflection losses by introducing a multilayer stack between the top and bottom cell which shows spectrally selective transmission/reflection behavior. The layer stack is designed and optimized by optical simulations using transfer matrix method and a genetic algorithm. The incident sun light is split into a direct part and an isotropic diffuse part. The tandem solar cell with interlayer shows an absolute improvement of short-circuit current density of 0.82 mA/cm^2.

OCIS codes: (310.4165) Multilayer design; (310.6805) Theory and design; (230.1480) Bragg reflectors; (350.6050) Solar energy.

References and links

1. J. H. Heo, S. H. Im, J. H. Noh, T. N. Mandal, C. S. Lim, J. A. Chang, Y. H. Lee, H. J. Kim, A. Sarkar, M. K. Nazeeruddin, M. Grätzel, and S. I. Seok, "Efficient Inorganic-Organic Hybrid Heterojunction Solar Cells Containing Perovskite Compound and Polymeric Hole Conductors," Nat. Photonics **7**(6), 486–491 (2013).
2. H. S. Kim, C. R. Lee, J. H. Im, K. B. Lee, T. Moehl, A. Marchioro, S. J. Moon, R. Humphry-Baker, J. H. Yum, J. E. Moser, M. Grätzel, and N. G. Park, "Lead Iodide Perovskite Sensitized All-Solid-State Submicron Thin Film Mesoscopic Solar Cell With Efficiency Exceeding 9%," Sci. Rep. **2**(1), 591 (2012).
3. M. M. Lee, J. Teuscher, T. Miyasaka, T. N. Murakami, and H. J. Snaith, "Efficient Hybrid Solar Cells Based on Meso-Superstructured Organometal Halide Perovskites," Science **338**(6107), 643–647 (2012).
4. W. S. Yang, J. H. Noh, N. J. Jeon, Y. C. Kim, S. Ryu, J. Seo, and S. I. Seok, "High-performance photovoltaic perovskite layers fabricated through intramolecular exchange," Science **348**(6240), 1234–1237 (2015).
5. T. P. White, N. N. Lal, and K. R. Catchpole, "Tandem Solar Cells Based on High-Efficiency c-Si Bottom Cells: Top Cell Requirements for >30% Efficiency," IEEE J. Photovolt. **4**(1), 208–214 (2014).
6. N. N. Lal, T. P. White, and K. R. Catchpole, "Optics and Light Trapping for Tandem Solar Cells on Silicon," IEEE J. Photovolt. **4**(6), 1380–1386 (2014).
7. K. A. Bush, A. F. Palmstrom, Z. J. Yu, M. Boccard, R. Cheacharoen, J. P. Mailoa, D. P. McMeekin, R. L. Z. Hoye, C. D. Bailie, T. Leijtens, I. M. Peters, M. C. Minichetti, N. Rolston, R. Prasanna, S. Sofia, D. Harwood, W. Ma, F. Moghadam, H. J. Snaith, T. Buonassisi, Z. C. Holman, S. F. Bent, and M. D. McGehee, "23.6%-efficient monolithic perovskite/silicon tandem solar cells with improved stability," Nat. Energy **2**(4), 17009 (2017).
8. S. Albrecht, M. Saliba, J. P. Correa-Baena, F. Lang, K. Kegelmann, M. Mews, L. Steier, A. Abate, J. Rappich, L. Korte, R. Schlatmann, M. K. Nazeeruddin, A. Hagfeldt, M. Grätzel, and B. Rech, "Monolithic Perovskite/Silicon-Heterojunction Tandem Solar Cells Processed at Low Temperature," Energy Environ. Sci. **9**(1), 81–88 (2016).
9. J. P. Mailoa, C. D. Bailie, E. C. Johlin, E. T. Hoke, A. J. Akey, W. H. Nguyen, M. D. McGehee, and T. Buonassisi, "2-Terminal Perovskite/Silicon Multijunction Solar Cell Enabled by a Silicon Tunnel Junction," Appl. Phys. Lett. **106**(12), 121105 (2015).
10. K. Yoshikawa, H. Kawasaki, W. Yoshida, T. Irie, K. Konishi, K. Nakano, T. Uto, D. Adachi, M. Kanematsu, H. Uzu, and K. Yamamoto, "Silicon heterojunction solar cell with interdigitated back contacts for a photoconversion efficiency over 26%," Nat. Energy **2**(5), 17032 (2017).

#327732 https://doi.org/10.1364/OE.26.00A750
Journal © 2018 Received 5 Apr 2018; revised 24 May 2018; accepted 7 Jun 2018; published 24 Jul 2018

Optics EXPRESS

11. M. Taguchi, A. Yano, S. Tohoda, K. Matsuyama, Y. Nakamura, T. Nishiwaki, K. Fujita, and E. Maruyama, "24.7% Record Efficiency HIT Solar Cell on Thin Silicon Wafer," IEEE J. Photovolt. **4**(1), 96–99 (2014).
12. S. D. Stranks and H. J. Snaith, "Metal-halide perovskites for photovoltaic and light-emitting devices," Nat. Nanotechnol. **10**(5), 391–402 (2015).
13. L. K. Ono, E. J. Juarez-Perez, and Y. Qi, "Progress on Perovskite Materials and Solar Cells with Mixed Cations and Halide Anions," ACS Appl. Mater. Interfaces **9**(36), 30197–30246 (2017).
14. W. Zhang, G. E. Eperon, and H. J. Snaith, "Metal halide perovskites for energy applications," Nat. Energy **1**(6), 16048 (2016).
15. D. T. Grant, K. R. Catchpole, K. J. Weber, and T. P. White, "Design guidelines for perovskite/silicon 2-terminal tandem solar cells: an optical study," Opt. Express **24**(22), A1454–A1470 (2016).
16. Y. M. Yang, Q. Chen, Y. T. Hsieh, T. B. Song, N. D. Marco, H. Zhou, and Y. Yang, "Multilayer Transparent Top Electrode for Solution Processed Perovskite/Cu(In,Ga)(Se,S)2 Four Terminal Tandem Solar Cells," ACS Nano **9**(7), 7714–7721 (2015).
17. Y. Jiang, I. Almansouri, S. Huang, T. Young, Y. Li, Y. Peng, Q. Hou, L. Spiccia, U. Bach, Y. Cheng, M. A. Green, and A. Ho-Baillie, "Optical analysis of perovskite/silicon tandem solar cells," J. Mater. Chem. C Mater. Opt. Electron. Devices **4**(24), 5679–5689 (2016).
18. G. E. Eperon, M. T. Hörantner, and H. J. Snaith, "Metal halide perovskite tandem and multiple-junction photovoltaics," Nat. Rev. Chem. **1**(12), 0095 (2017).
19. M. T. Hörantner and H. J. Snaith, "Predicting and optimising the energy yield of perovskite-on-silicon tandem solar cells under real world conditions," Energy Environ. Sci. **10**(9), 1983–1993 (2017).
20. G. W. P. Adhyaksa, E. Johlin, and E. C. Garnett, "Nanoscale Back Contact Perovskite Solar Cell Design for Improved Tandem Efficiency," Nano Lett. **17**(9), 5206–5212 (2017).
21. C. D. Bailie and M. D. McGehee, "High-efficiency tandem perovskite solar cells," MRS Bull. **40**(08), 681–686 (2015).
22. M. Jaysankar, W. Qiu, M. van Eerden, T. Aernouts, R. Gehlhaar, M. Debucquoy, U. W. Paetzold, and J. Poortmans, "Four-Terminal Perovskite/Silicon Multijunction Solar Modules," Adv. Energy Mater. **7**(15), 1602807 (2017).
23. M. Filipič, P. Löper, B. Niesen, S. De Wolf, J. Krč, C. Ballif, and M. Topič, "CH3NH3PbI3 perovskite / silicon tandem solar cells: characterization based optical simulations," Opt. Express **23**(7), A263–A278 (2015).
24. S. Albrecht, M. Saliba, J. Correa-Baena, K. Jäger, L. Korte, A. Hagfeldt, M. Grätzel, and B. Rech, "Towards optical optimization of planar monolithic perovskite/silicon-heterojunction tandem solar cells," J. Opt. **18**(6), 064012 (2016).
25. J. Pla, M. Tamasi, R. Rizzoli, M. Losurdo, E. Centurioni, C. Summonte, and F. Rubinelli, "Optimization of ITO layers for applications in a-Si/c-Si heterojunction solar cells," Thin Solid Films **425**(1-2), 185–192 (2003).
26. Z. C. Holman, M. Filipič, A. Descoeudres, S. De Wolf, F. Smole, M. Topič, and C. Ballif, "Infrared light management in high-efficiency silicon heterojunction and rear-passivated solar cells," J. Appl. Phys. **113**(1), 013107 (2013).
27. A. Hoffmann, K. Bittkau, C. Zhang, M. Meier, R. Carius, and U. Rau, "Photon Tunneling in Tandem Solar Cells With Intermediate Reflector," IEEE J. Photovolt. **6**(3), 597–603 (2016).
28. A. Bielawny, C. Rockstuhl, F. Lederer, and R. B. Wehrspohn, "Intermediate reflectors for enhanced top cell performance in photovoltaic thin-film tandem cells," Opt. Express **17**(10), 8439–8446 (2009).
29. P. G. O'Brien, A. Chutinan, K. Leong, N. P. Kherani, G. A. Ozin, and S. Zukotynski, "Photonic crystal intermediate reflectors for micromorph solar cells: A comparative study," Opt. Express **18**(5), 4478–4490 (2010).
30. V. M. Emelyanov, N. A. Kalyuzhnyy, S. A. Mintairov, M. Z. Shvarts, and V. M. Lantratov, "Multijunction GaInP/GaInAs/Ge Solar Cells with Bragg Reflectors," Semiconductors **44**(12), 1600–1605 (2010).
31. A. Mellor, N. P. Hylton, S. A. Maier, and N. Ekins-Daukes, "Interstitial light-trapping design for multi-junction solar cells," Sol. Energy Mater. Sol. Cells **159**, 212–218 (2017).
32. A. Hoffmann, U. W. Paetzold, C. Zhang, T. Merdzhanova, A. Lambertz, C. Ulbrich, K. Bittkau, and U. Rau, "Advancing tandem solar cells by spectrally selective multilayer intermediate reflectors," Opt. Express **22**(S5 Suppl 5), A1270–A1277 (2014).
33. P. Buehlmann, J. Bailat, D. Dominé, A. Billet, F. Meillaud, A. Feltrin, and C. Ballif, "In situ silicon oxide based intermediate reflector for thin–film silicon micromorph solar cells," Appl. Phys. Lett. **91**(14), 143505 (2007).
34. A. Lambertz, T. Grundler, and F. Finger, "Hydrogenated amorphous silicon oxide containing a microcrystalline silicon phase and usage as an intermediate reflector in thin–film silicon solar cells," J. Appl. Phys. **109**(11), 113109 (2011).
35. A. Richter, V. Smirnov, A. Lambertz, K. Nomoto, K. Welter, and K. Ding, "Versatility of doped nanocrystalline silicon oxide for applications in silicon thin-film and heterojunction solar cells," Sol. Energy Mater. Sol. Cells **174**, 96–201 (2018).
36. Y. Wu, D. Yan, J. Peng, T. Duong, Y. Wan, S. P. Phang, H. Shen, N. Wu, C. Barugkin, X. Fu, S. Surve, D. Grant, D. Walter, T. P. White, K. R. Catchpole, and K. J. Weber, "Monolithic perovskite/silicon-homojunction tandem solar cell with over 22% efficiency," Energy Environ. Sci. **10**(11), 2472–2479 (2017).
37. P. S. C. Schulze, A. J. Bett, K. Winkler, A. Hinsch, S. Lee, S. Mastroianni, L. E. Mundt, M. Mundus, U. Würfel, S. W. Glunz, M. Hermle, and J. C. Goldschmidt, "Novel Low-Temperature Process for Perovskite Solar Cells with a Mesoporous TiO_2 Scaffold," ACS Appl. Mater. Interfaces **9**(36), 30567–30574 (2017).

Optics EXPRESS

38. H. Tan, A. Jain, O. Voznyy, X. Lan, F. P. García de Arquer, J. Z. Fan, R. Quintero-Bermudez, M. Yuan, B. Zhang, Y. Zhao, F. Fan, P. Li, L. N. Quan, Y. Zhao, Z.-H. Lu, Z. Yang, S. Hoogland, and E. H. Sargent, "Efficient and stable solution-processed planar perovskite solar cells via contact passivation," Science **355**(6326), 722–726 (2017).
39. J. H. Kim, P. W. Liang, S. T. Williams, N. Cho, C. C. Chueh, M. S. Glaz, D. S. Ginger, and A. K.-Y. Jen, "High-Performance and Environmentally Stable Planar Heterojunction Perovskite Solar Cells Based on a Solution-Processed Copper-Doped Nickel Oxide Hole-Transporting Layer," Adv. Mater. **27**(4), 695–701 (2015).
40. M. Saliba, T. Matsui, J.-Y. Seo, K. Domanski, J.-P. Correa-Baena, M. K. Nazeeruddin, S. M. Zakeeruddin, W. Tress, A. Abate, A. Hagfeldt, and M. Grätzel, "Cesium-containing triple cation perovskite solar cells: improved stability, reproducibility and high efficiency," Energy Environ. Sci. **9**(6), 1989–1997 (2016).
41. S. J. Byrnes, "Multilayer optical calculations," *https://arxiv.org/abs/1603.02720*.
42. P. B. Johnson and R. W. Christy, "Optical Constants of the Noble Metals," Phys. Rev. B **6**(12), 4370–4379 (1972).
43. G. E. Jellison, Jr., "Optical functions of silicon determined by two-channel polarization modulation ellipsometry," Opt. Mater. **1**(1), 41–47 (1992).
44. R. Perez, R. Stewart, C. Arbogast, R. Seals, and J. Scott, "An anisotropic hourly diffuse radiation model for sloping surfaces: description, performance validation, site dependency evaluation," Sol. Energy **36**(6), 481–497 (1986).
45. P. G. Loutzenhiser, H. Manz, C. Felsmann, P. A. Strachan, T. Frank, and G. M. Maxwell, "Empirical validation of models to compute solar irradiance on inclined surfaces for building energy simulation," Sol. Energy **81**(2), 254–267 (2007).
46. R. L. Haupt and S. E. Haupt, *Practical Genetic Algorithms, 2nd Edition* (John Wiley & Sons, Inc, 2004).
47. L. Mazzarella, M. Werth, K. Jäger, M. Jošt, L. Korte, S. Albrecht, R. Schlatmann, and B. Stannowski, "Infrared photocurrent management in monolithic perovskite/silicon heterojunction tandem solar cells by using a nanocrystalline silicon oxide interlayer," Opt. Express **26**(10), A487–A497 (2018).
48. B. C. Duck, R. B. Dunbar, O. Lee, K. F. Anderson, T. W. Jones, G. J. Wilson, and C. J. Fell, "Energy Yield Potential of Perovskite-Silicon Tandem Devices," in 43rd IEEE Photovoltaic Specialists Conference (PVSC) (2016), pp. 1624–1629.
49. R. Santbergen, R. Mishima, T. Meguro, M. Hino, H. Uzu, J. Blanker, K. Yamamoto, and M. Zeman, "Minimizing optical losses in monolithic perovskite/c-Si tandem solar cells with a flat top cell," Opt. Express **24**(18), A1288–A1299 (2016).

1. Introduction

The rapid increase in power conversion efficiency of metal halide perovskite solar cells (PSC) [1–4] and their high optical band-gap make these devices to attractive candidates for top cells for crystalline silicon (c-Si) solar cell technology [5–9]. Silicon heterojunction (SHJ) solar cells show very high efficiencies, even higher than silicon homojunction solar cells [10,11]. Recently, many different process technologies and layer combinations were investigated for PSC as this technology still needs much work in order to optimize the device performance [12–14]. In particular, a lot of research is currently ongoing to identify optimal electron and hole transport layers [15–17].

When looking for a tandem cell application, one has to distinguish between monolithic two-terminal devices and four-terminal devices [17–23]. The big advantage of the two-terminal device is that only one matching box is necessary for the module application. In contrast, the four-terminal device allows that both cells can be individually driven at their respective maximum power point, whereas current matching has to be taken into account for the two-terminal concept. From an optical point of view, one has to take care about any layer between the top cell absorber and the bottom cell absorber for both tandem device concepts to achieve a good optical matching. In particular, layers with refractive indices significantly lower than those of the absorber layers cause reflection losses for light with photon energies lower than the band gap of the top cell absorber [15,23,24].

In case of the four-terminal architecture, two contact layers with sufficiently low sheet resistance need to be deposited between the top cell and bottom cell absorber in order to collect the charge carriers from both cells. Such layers typically show significant absorption losses. Additionally, the mechanical stacking demands for a transparent medium like glass, air or an index matching liquid which separates these contact layers. Therefore, an optically thick region with low refractive index and high absorption can hardly be avoided here.

Optics EXPRESS

The two-terminal architecture offers a big advantage. For SHJ solar cells, indium tin oxide (ITO) layers were commonly applied at the front contact due to their good combination of electrical and optical properties [25,26]. Although ITO as well as commonly used charge selective contacts for the PSC still exhibit low refractive indices, such layers are comparatively thin, in particular in the case of a tandem device, where lateral charge transport is not required. Therefore, the optical light coupling between top and bottom cell is possible in terms of coherent light coupling [27]. This allows the design of photonic layer architectures which partly compensate reflection losses of impinging light [28–32].

In this paper, we present the optical design of a spectrally selective interlayer (IL) stack based on hydrogenated microcrystalline silicon oxide (µc-SiO_x:H) layers with various oxygen contents which form a reduced dielectric Bragg reflector that is sandwiched between top and bottom cell [32–34]. It will be shown that without this layer stack, the reflection losses dominantly occur in a restricted spectral range. The introduction of the IL significantly reduces the overall reflection losses. We will demonstrate that the short-circuit current density (J_{SC}) of a two-terminal PSC/SHJ tandem solar cell can be increased by 0.82 mA/cm^2 when applying our IL. This value is 0.18 mA/cm^2 higher compared to the optimized layer stack including just a single µc-SiO_x:H interlayer due to improved spectral matching between top and bottom cell. Our study includes a cover glass on top of the tandem cell and accounts for ambient light illumination including the diffusive part of incident sun light. We will show that the tandem solar cell including the IL outperforms the reference tandem solar cell without IL for any angle of incident sun light.

2. Methodology

2.1 Device structure

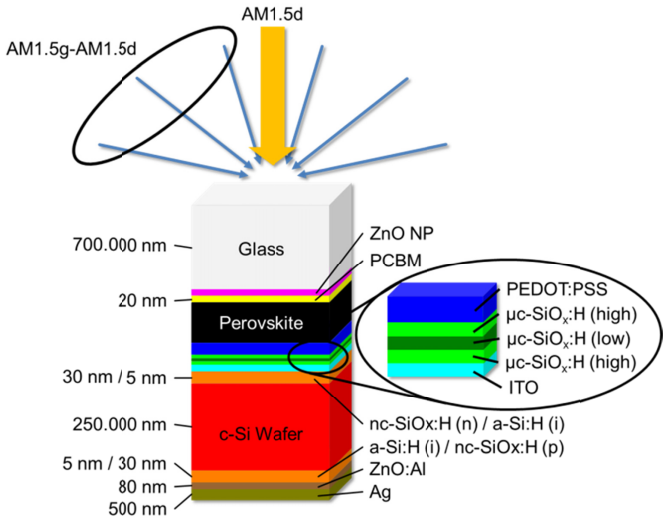

Fig. 1. Illustration of the layer stack used for the study. Thicknesses were provided for those layers, where the thickness was not varied during the optimization procedure. The arrows at the top illustrate the assumed incident sun light with AM1.5d at normal incidence and the isotropic impinging diffuse part of the AM1.5g.

We focus our study to SHJ bottom solar cells applying hydrogenated amorphous silicon (a-Si:H) passivation layers and doped hydrogenated, nanocrystalline silicon oxide (nc-SiO_x:H) charge carrier selective contacts as such layers have a high optical transparency and the solar cells reveal reasonably high efficiencies [35]. As the a-Si:H layers are limiting the temperature for any further deposition process, any material which requires temperatures higher than 200 °C is no option for the PSC. As one example, the commonly used TiO_x as

electron transport layer for PSC is often annealed at temperatures of 400 °C [36], although lower process temperatures were reported [37,38]. Besides other possible materials that do not require such high temperatures, Poly(3,4-ethylenedioxythiophene):poly(styrenesulfonate) (PEDOT:PSS) is used as hole transport layer for our simulation study as the processing is simple and flexible, resulting in reasonable efficiencies [39]. As electron transport layer, we use [6,6]-phenyl-C_{61}-butyric acid methyl ester (PCBM). The whole layer stack is illustrated in Fig. 1.

As back reflector, an 80 nm thick aluminum doped zinc oxide (ZnO:Al) and a 500 nm thick silver (Ag) layer stack is assumed. The c-Si absorber is passivated at both sides with 5 nm thick a-Si:H. 30 nm thick p-doped and n-doped nc-SiO_x:H was assumed at the back and front side of the 250 µm thick silicon wafer as carrier selective contact layers for the bottom cell, respectively. The bottom cell is complemented with an ITO layer. The IL consists of three µc-SiO_x:H layers with high, low and high refractive index, respectively.

For the top cell, PEDOT:PSS is assumed as hole transport layer, followed by a quadruple cation perovskite layer with a bandgap energy of 1.65 eV, which can be prepared similar to a previously published recipe [40] with added guanidinium iodide. Details about this process will be published elsewhere. The perovskite layer is coated with a 20 nm thick PCBM as electron transport layer, capped with a buffer layer consisting of ZnO nanoparticles (ZnO NP) and a 700 µm thick glass cover sheet.

During the study, the thicknesses of the ITO, the individual layers of the IL, the PEDOT:PSS, the perovskite and the ZnO NP were varied in order to achieve the highest possible J_{SC}. All interfaces were assumed to be flat.

2.2 Simulation

The optical design of the layer stack is done based on the transfer matrix method (TMM) [41]. The complex refractive indices for Ag and c-Si were taken from literature [42,43]. The values for all other materials were experimentally determined by a combination of reflection/transmission measurement, spectroscopic ellipsometry and photo-thermal deflection spectroscopy on reference samples. All layers with silicon and silicon-based alloys were deposited by plasma enhanced chemical vapor deposition, ITO and back contact by sputtering and the layers of the top solar cell by spin coating from liquid phase. For the most important layers for the optical matching condition between top cell and bottom cell, the wavelength dependent refractive indices n (a) and extinction coefficients k (b) were shown in Fig. 2. The wavelength of 750 nm is depicted as dotted vertical line. This wavelength almost equals the optical bandgap of the perovskite layer and, therefore, represents the spectral region where the optical matching between top and bottom cell is mostly relevant.

At this wavelength, the two absorber layers have the highest refractive indices n (3.71 for c-Si and 2.44 for perovskite) with respect to the other materials, whereas the two layers that extract the charge carriers, PEDOT:PSS and ITO, have the lowest refractive indices (1.54 and 1.71, respectively). As interlayers, the high refractive silicon oxide alloy with lower oxygen content and a refractive index of 2.17 at a wavelength of 750 nm was assumed. The second component of the IL consists of a µc-SiO_x:H with higher oxygen content and, therefore, lower refractive index of 1.77 at a wavelength of 750 nm.

Optics EXPRESS

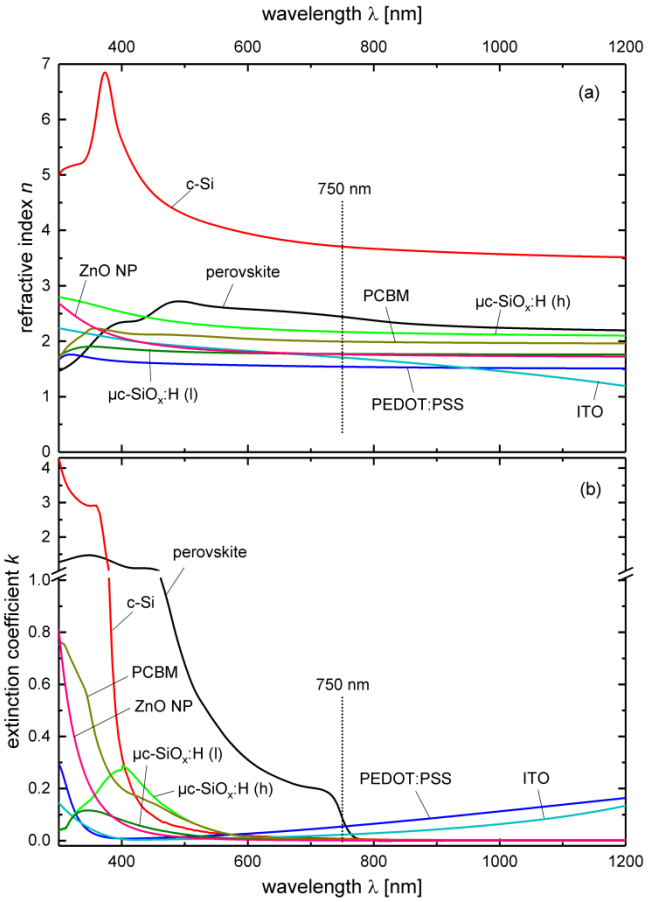

Fig. 2. (a) Refractive index n and (b) extinction coefficient k for the most relevant materials for the optical matching condition between top and bottom cell. The vertical dotted lines depict the wavelength which corresponds to the optical bandgap of the perovskite.

For the TMM simulation, the 700 µm thick glass sheet as well as the 250 µm thick c-Si were assumed as incoherent layers, whereas all other layers were assumed as coherent layers. As the illumination conditions are of major importance for tandem solar cells, the incident light is assumed to consist of a direct and a diffusive component. For the direct light, the AM1.5d spectrum is assumed to impinge along the surface normal. The diffuse part of the sun light (AM1.5g-AM1.5d) is spread over nine angles of incidence, 0°-80° in steps of 10°. The intensities for each angle were weighted in a way to assume an isotropic illumination characteristic from the upper half space. This illumination and the glass cover sheet were chosen to represent a much more realistic condition for real application compared to common approaches. More advanced sky models split the sky into a circumsolar region, a near-horizon region and the remaining region. Although those models describe the solar irradiance more accurately compared to the isotropic assumption [44,45], the deviations are small compared to regional variations of the sun spectrum and the impact of mounting angles on the incident solid angle range. The absorptance in each layer was extracted and the corresponding J_{SC} of the tandem solar cell calculated from the minimum of the charge carrier generation in both absorber layers. By applying a genetic algorithm [46], the layer thicknesses were optimized to achieve the maximal J_{SC}. The advantages of a genetic algorithm are its ability to deal with multiple variables and its applicability to parallel processing. Furthermore, a genetic algorithm does not need derivative information for optimization. The population size,

selection fraction, mutation rate and number of iterations were chosen to be 450, 0.65, 0.08 and 400, respectively, and the generated J_{SC} is taken as fitness value. For the ZnO NP, PEDOT:PSS and ITO layers, lower boundaries for the thickness were defined as 35 nm, 20 nm and 35 nm, respectively.

3. Results and discussions

This section is structured as follows. First, we present an optical loss analysis for the optimized reference tandem solar cell without IL stack. We will demonstrate that reflection losses in the spectral range from 600 nm – 900 nm play a major role in the limitation of the device. Next, we will introduce the three-layer stack as IL between the top and bottom cell. We will demonstrate that this IL3 causes a significant reduction of reflection losses which increases the absorptance in both, top cell and bottom cell absorber. This will be complemented by a direct comparison of absorptance and solar cell reflectance for the layer stacks with and without IL. For comparison, we also designed a tandem solar cell with a single IL1 [47] consisting of the μc-SiO_x:H layer with higher refractive index. Our study will be finalized by a quantification of the effect of the IL3 on the J_{SC} as a function of the angle of incidence.

Table 1. Layer thicknesses resulting from the optimization of the tandem solar cell without and with IL

interlayer	ITO	IL1	IL2	IL3	PEDOT:PSS	perovskite	ZnO NP
without	35 nm	NA	NA	NA	26 nm	220 nm	35 nm
with IL1	35 nm	99 nm	NA	NA	35 nm	251 nm	41 nm
with IL3	36 nm	57 nm	128 nm	95 nm	21 nm	256 nm	36 nm

Table 1 summarizes the layer thicknesses that were determined by the optimization procedure of the genetic algorithm for the tandem solar cell without and with IL. The order of the columns follows the order of the layers in the tandem solar cell stack in the direction from the bottom cell to the front contact. IL1 and IL3 represent the high refractive μc-SiO_x:H, IL2 shows the thickness of the low refractive μc-SiO_x:H layer. Note that the optimized thicknesses for the ITO, PEDOT:PSS and ZnO NP layers were very close to the lower boundaries of 35 nm, 20 nm and 35 nm, respectively.

Figure 3(a) shows the optical loss analysis for the tandem solar cell stack without IL. Any colored area corresponds to the amount of incident light that is absorbed in the related layer. The top and bottom cell absorber, perovskite and c-Si, were represented by the black and red color, respectively. The absorptance in the ZnO NP and PCBM layers at the front side of the tandem solar cell were shown in magenta and green, respectively. PEDOT:PSS is shown as dark blue and ITO as light blue area. The optical losses within the passivation and charge carrier selective contacts of the SHJ bottom cell were represented together in orange. The absorptance in the back reflector stack (ZnO:Al/Ag) is shown in dark yellow. The white area corresponds to light that is reflected by the whole tandem solar cell stack. Only the black and red areas correspond to the J_{SC}. Any other colored area contributes to parasitic absorption losses.

The parasitic absorption in the short-wavelength range (wavelengths $\lambda<600$ nm) is dominantly determined by the absorptance in the ZnO NP and PCBM layers, which correspond to losses in J_{SC} of 0.52 mA/cm^2 and 0.77 mA/cm^2, respectively. For light with $\lambda>600$ nm, the main contribution to the parasitic absorption is given by the absorption losses in the PEDOT:PSS layer (1.13 mA/cm^2) followed by ITO (0.67 mA/cm^2). Absorption losses originating from other layers are negligible. A huge contribution to optical losses arises from solar cell reflectance. Reflection losses in the long wavelength range ($\lambda>1000$ nm) can hardly be avoided with the assumed flat interfaces due to the weak absorption in both absorber layers. A remarkable reflection loss occurs in the spectral range 600 nm$<\lambda<$900 nm with a well-pronounced dip. This reflection loss originates from the significant steps in the refractive

Optics EXPRESS

indices along the transition from the top cell to the bottom cell, mainly the perovskite/PEDOT:PSS interface and the ITO/Si interface.

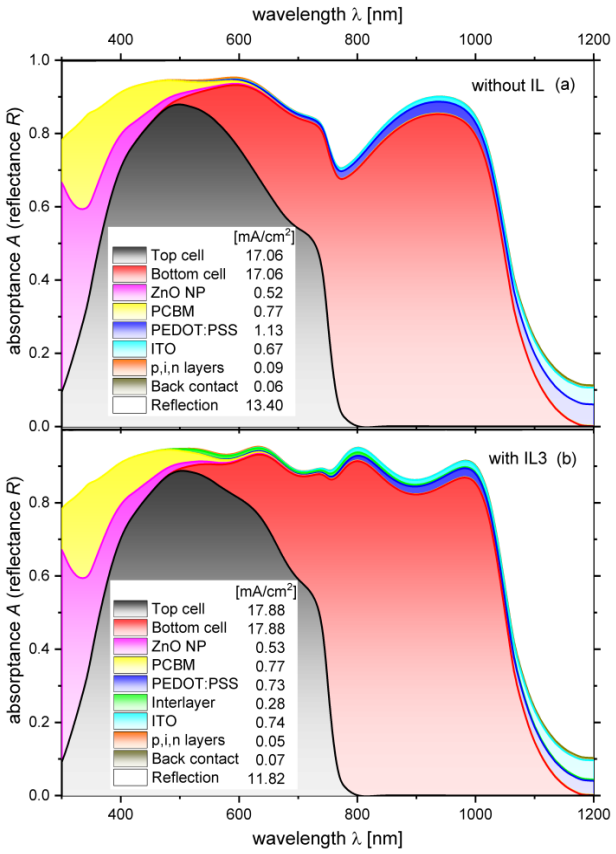

Fig. 3. Optical loss analysis for the tandem solar cell stack without IL (a) and with IL3 (b). The colored areas illustrate the distribution of light absorption over the involved layers. The white area represents the reflected light. The correlated J_{SC} values were provided in the legend

Another issue can be seen in the spectral range from 500 nm<λ<750 nm. Here, the perovskite layer can still absorb photons but obviously not fully. Instead, a significant amount of incident light is absorbed in the c-Si wafer. Due to the higher open-circuit voltage of the perovskite top cell, a photon that is absorbed in the c-Si causes higher thermalization losses compared to a photon that is absorbed in the perovskite. Therefore, it would be advantageous to improve the absorptance in the perovskite layer in this spectral range. In this case, it would mean that a good optical interlayer should (i) lead to a decrease of the absorptance in the c-Si in the spectral range 500 nm<λ<750 nm by increasing the absorptance in the top cell, (ii) increase the absorptance in the c-Si wafer in the spectral range 750 nm<λ<900 nm by a higher transmittance of impinging light to the bottom cell and (iii) reduce the overall solar cell reflectance in the spectral range 600 nm<λ<900 nm.

The optical loss analysis for the tandem solar cell stack with IL3 is shown in Fig. 3(b) with the same color code as in Fig. 3(a). The additional interlayers were represented in yellow. Compared to the tandem cell without IL, the reflection losses in the spectral range 600 nm<λ<900 nm appears to be reduced when the IL3 is implemented into the layer stack and layer thicknesses optimized. It can also be seen that parasitic absorption losses still only play a minor role in this spectral range suggesting that the absorptance, and thereby the *EQE*, of the c-Si wafer is increased. In order to compare the layer stacks better, the overall solar cell

Optics EXPRESS

reflectance *R* for the layer stack without IL (solid line), with IL1 (dotted lines) and with IL3 (dashed line) is shown in Fig. 4(a). The absorptance of the top cell (black lines) and bottom cell (red lines) are illustrated in Fig. 4(b) for the tandem solar cell without IL (solid lines), with IL1 (dotted lines) and with IL3 (dashed lines).

Obviously, a significant reduction of the solar cell reflectance in the range 600 nm<λ<900 nm is achieved by introducing an IL between the top and bottom cell. Outside this spectral range, both reflectance curves appear very similar. This demonstrates a significant improvement of the utilization of sun light. In order to evaluate how this reduced solar cell reflectance is affecting the performance of the tandem solar cell, the absorptance of top and bottom cell were plotted together in Fig. 4(b) for the tandem solar cells with and without IL.

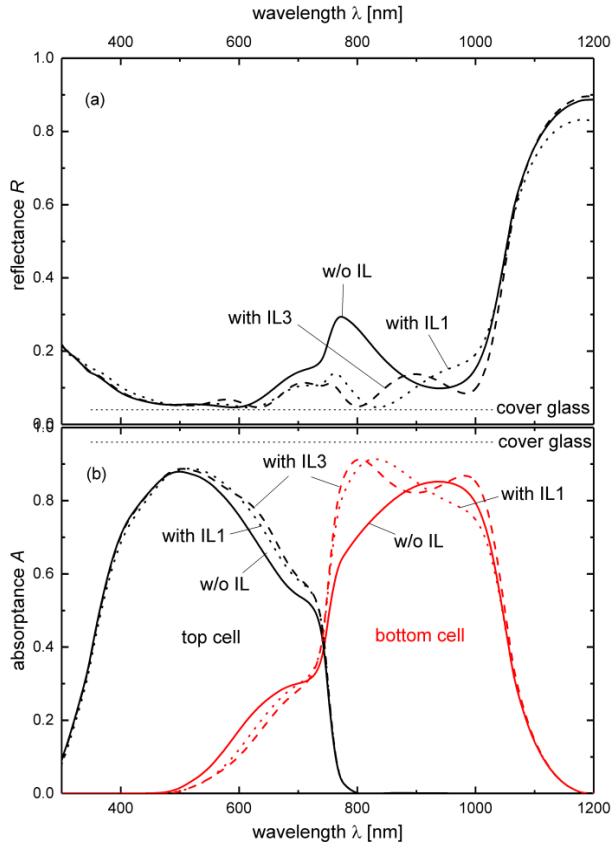

Fig. 4. (a) Solar cell reflectance as a function of the wavelength of incident light and (b) absorptance of top cell (black) and bottom cell (red). The tandem solar cell without IL is represented as solid lines, the tandem solar cell with IL1 and IL3 as dotted and dashed lines, respectively. The horizontal line represents the expected reflectance (maximal achievable absorptance) that originates from the front cover glass.

The absorptance in the bottom cell is significantly reduced in the spectral range 500 nm<λ<750 nm. Simultaneously, the absorptance in the top cell is significantly increased in the same spectral range. This is caused by either the reflectance of impinging light at the IL or the larger thickness of the perovskite layer in the case of the tandem solar cell with IL (256 nm instead of 220 nm, cf. Table 1). In the spectral range 750 nm<λ<850 nm, a strong increase in the absorptance of the bottom cell is found. This increase is directly related to the decrease in solar cell reflectance and demonstrates the strong spectral selectivity of the IL. Impinging light with 500 nm<λ<750 nm is efficiently reflected, whereas impinging light with 750 nm<λ<850 nm is efficiently transmitted. Thus, the designed IL behaves as desired. This

Optics EXPRESS

behavior leads to an increase in the J_{SC} of the tandem solar cell with IL compared to the tandem solar cell without IL. The corresponding values are summarized in Table 2.

Table 2. Short-circuit current densities J_{SC} and integrated reflection losses of the tandem solar cells without and with intermediate layers

interlayer	short-circuit current density J_{SC}	reflection losses 600 nm – 900 nm
without	17.06 mA/cm^2	3.25 mA/cm^2
with IL1	17.70 mA/cm^2	1.67 mA/cm^2
with IL3	17.88 mA/cm^2	1.70 mA/cm^2

The J_{SC} of the tandem solar cell without IL was determined to be 17.06 mA/cm^2. The integrated reflection losses in the spectral range 600 nm<λ<900 nm corresponds to a short-circuit current density of 3.25 mA/cm^2. The tandem solar cell with IL1 shows a J_{SC} and reflection losses of 17.70 mA/cm^2 and 1.67 mA/cm^2, respectively. For the tandem solar cell with IL, the J_{SC} and the reflection losses were 17.88 mA/cm^2 and 1.70 mA/cm^2, respectively. This means that the IL3 leads to a reduction of reflection losses by 1.55 mA/cm^2 and an increase in J_{SC} by 0.82 mA/cm^2 compared to the tandem cell without IL. Assuming that the reduction of reflection losses is distributed equally to top and bottom cell absorber, remaining the current matching condition, the J_{SC} is expected to be increased by half of the value that the reflection losses are reduced. This condition is almost fulfilled. For the tandem solar cell with IR1, the reflection losses are slightly lower compared to the tandem solar cell with IR3 but the achieved J_{SC} is also lower. This means that the spectral selectivity of the IR1 is lower than that of the IR3.

Another issue that needs to be addressed is the dependency of the device performance on the angle of incidence. On the one hand, elongated path lengths of impinging light in the top cell absorber due to oblique angles impact the amount of absorbed photons therein. Therefore, the spectral density that reaches the bottom cell is influenced by the angle of incidence. This probably disturbs the current matching condition and induces significant losses in the device [48]. On the other hand, a multilayered IL, as introduced in our study, makes the situation even more relevant. The discussed effects of the IL on the solar cell reflectance and *EQE* of top and bottom cell depend on the angle at which light impinges the IL.

Figure 5 presents the angular dependency of the J_{SC} of the tandem solar cells without (black lines) and with (red lines) IL3 for diffuse irradiance (solid) and specular irradiance (dotted). Note, that in case of the diffuse irradiance the incident solar spectrum is split into the direct part and the diffuse part. Only the direct part of incident solar irradiance is affected by the angle of incidence, whereas the diffuse part is always assumed to illuminate the solar cells isotropically from the upper half space. In case of the specular irradiance, the same solar cell stacks were illuminated with the full AM1.5g spectrum at the angle of incidence. It can be seen that, although the decrease in J_{SC} with the angle of incidence is slightly stronger for the tandem cell with IL3, the absolute value of the J_{SC} remains higher over the whole angular regime compared to the tandem cell without IL. This means that the introduction of an IL3 between the top and bottom cell leads to an improvement in J_{SC} at any angle of incidence making this concept highly relevant for application. Furthermore, it can be seen that the angular dependency is stronger for the situation with specular irradiance. In other words, the tandem solar cells are more robust against the angle of incidence when the diffuse part of solar irradiance is taken into account.

Optics EXPRESS

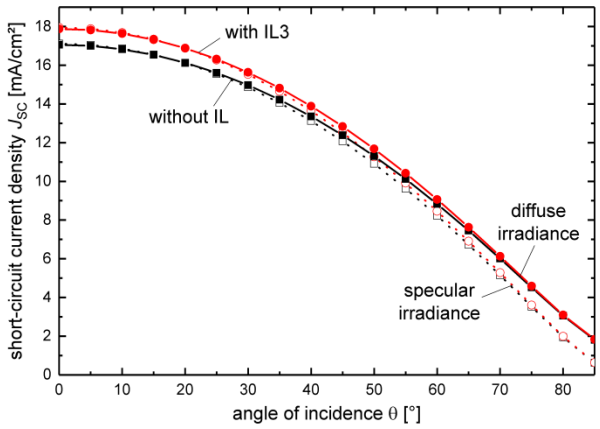

Fig. 5. Short-circuit current density J_{SC} as a function of the wavelength of incident light. The result for the tandem solar cell without IL is shown in black lines, those for the tandem solar cell with IL3 as red lines. Solid lines show the results for diffuse irradiance, dotted lines the results for specular irradiance.

Future work could implement a back side texture to the c-Si bottom cell to increase the absorptance in the long-wavelength region [49]. Furthermore, electrical properties of the involved materials and interfaces should be better understood to find the optimal layer combination, in particular for the top cell.

4. Conclusion

We have shown that reflection losses in the spectral range 600 nm<λ<900 nm play a crucial role for the performance of PSC/SHJ tandem solar cells. These losses originate at the optical transition from the top cell to the bottom cell and are mainly caused by the low refractive indices of PEDOT:PSS and ITO. In order to compensate these losses, we designed a multilayer stack which is sandwiched between top and bottom solar cell and consists of an alternating series of high, low and high refracting μc-SiO_x:H. Applying this interlayer, the *EQE* of both, top and bottom solar cell, is significantly improved while reducing the solar cell reflectance. The IL acts as a spectrally selective photonic component that reflects light with 500 nm<λ<750 nm and transmits light with 750 nm<λ<850 nm. The improved optical properties by the IL lead to an increase in J_{SC} by 0.82 mA/cm^2. We have demonstrated that the designed tandem solar cell with IL shows a higher J_{SC} compared to the reference tandem cell independent from the angle of incident light.

Funding

Bavarian Ministry for Economics, Media, Energy and Technology (project "Perowskit basierte Tandem-Solarzellen").

Acknowledgments

The authors thank S. Öz and S. Mathur for the development of the recipe for the perovskite absorber. D. Grabowski, A. Richter, A. Hoffmann, M. Steinhorst and O. Thimm are acknowledged for their experimental support to obtain the optical data of the layers.